A perturbation analysis of the unstable plastic flow pattern evolution in an aluminum alloy

Seung-Yong Yang [a], Wei Tong [b,*]

[a] *School of Mechanical Engineering, Korea University of Technology and Education, South Korea*
[b] *Department of Mechanical Engineering, Southern Methodist University, Dallas, TX 75275-0337, USA*

Abstract

In the tensile loading of sheet metals made from some polycrystalline aluminum alloys, a single deformation band appears inclined to the elongation axis in the early stage of deformation, and symmetric double bands are observed in the later stage. This evolution of spatial characteristics of such an unstable plastic flow pattern in a polycrystalline aluminum alloy has been analyzed by a perturbation method. A small number of slip modes are taken to describe the tensile strain. A rate-dependent constitutive equation is used for each slip mode to account for the interaction between dislocations and solute atoms in dynamic strain aging. Unconstrained and constrained models are used to impose appropriate loading conditions at the early and later deformation stages, respectively. Both plane-strain and plane-stress cases are considered. It is found out that the change of boundary conditions and material inhomogeneity during the course of plastic deformation are closely related to the evolution of spatial characteristics of shear band (the Portevin–Le Chatelier band) patterns observed in experiments.
© 2005 Elsevier Ltd. All rights reserved.

Keywords: Plasticity; Localization; Dynamic strain aging; Portevin–Le Chatelier band

1. Introduction

Plastic deformation of polycrystalline metals and alloys at ambient temperature is primarily related to the collective motion of dislocations along specific crystallographic directions on specific crystallographic

planes (Bassani, 1994). While the motion of dislocations is both spatially and temporally discrete at the microscopic level, the plastic flow behavior due to the collective motion of dislocations in a polycrystalline is usually smooth and homogenous at the macroscopic level. However, when the motion of dislocations is significantly affected by the alloying elements in a solid solution alloy (inducing the so-called dynamic strain aging effect), the macroscopic plastic flow can become discontinuous and localized into a narrow deformation band or region one at a time. It has been observed in a recent experimental investigation that the pattern of discontinuous or localized deformation bands (the *Portevin–Le Chatelier* or PLC bands) associated with dynamic strain aging in the uniaxial tension of polycrystalline aluminum alloys with periodic stress relaxations depends on the deformation stage (Li and Tong, 1999; Li, 2001). In their experiment, a compact aluminum tensile test coupon with a gauge size of 20 mm long, 4.6 mm wide and 1 mm thick was stretched quasi-statically at a nominal strain rate of 5×10^{-4} 1/s to final rupture. One of the flat surfaces of the tensile coupon was decorated with a fine black-and-white contrast pattern via direct ink printing and a series of digital images of the coupon gage section were acquired at a frame rate of 1 per 0.5% overall strain increment. The digital images were processed via image correlation to generate both cumulative and incremental strain mapping contours for characterizing the unstable plastic flow patterns developed in the aluminum tensile coupon (Tong, 1997, 1998; Smith et al., 1998). As an example, a total of 21 *incremental* axial strain contours of an AA6111-T4 tensile coupon after initial yielding and before final rupture are given in Fig. 1 (see Li, 2001 for more experimental details). As shown in Fig. 1, at the early stage of the tensile loading of the thin polycrystalline aluminum alloy sheet, localized deformation bands crossing the whole width of the specimen are oblique to the loading axis, and the nucleation and growth of the bands is discontinuous along the elongation axis. Multiple uncorrelated localized deformation bands were detected per load increment. At the later stage, however, symmetric double bands form to make seemingly perpendicular bands to the tensile axis, and the correlated bands nucleate and grow more or less consecutively per each stress relaxation and reload cycle.

Finite element simulations have been conducted to study the PLC band patterns by conventional plasticity or crystal plasticity models with dynamic aging effects (Becker, 1999; Zhang et al., 2001; Yang and Tong, 2001). Although simulations showed results somewhat qualitatively in agreement with experimental observations, the underlying mechanisms for the evolution of distinct localization patterns were not clear. Labbe et al. (1998) applied an instability analysis developed for single crystals to polycrystals assumed as super single crystals. In this paper, the evolution of the spatial characteristics of PLC band patterns has been studied by a perturbation analysis. A minimum number of macroscopic slip modes that are kinematically necessary are assumed to dominate the plastic flow in polycrystalline metals under tension, and plastic strain components are decomposed into the sum of shear strains associated with the small number of slip modes. A rate-dependent constitutive equation including the interaction between dislocations and solute atoms is used for each slip mode. The decomposition of arbitrary strain into strains associated with a small number of the slip modes has merit in simplifying kinematics of plastic deformation. Describing constitutive behavior for each slip mode would have more physical insight to investigate microscopic mechanisms of plasticity than using conventional macroscopic flow rules. Appropriate boundary conditions are imposed to account for the early and later deformation stages of polycrystalline metals in uniaxial tension. That is, at the early deformation stage, the compatibility condition between neighboring grains can be neglected, and each grain is assumed to be subjected to the same homogeneous stress. Thus the shear stress for all grains is assumed to be zero (unconstrained model). On the other hand, at the later deformation stage, the plastic hardening modulus is small. The equilibrium condition between grains can be neglected, and each grain is assumed to be subjected to the same homogeneous deformation. Thus the shear component of the rate of deformation tensor is assumed to vanish (constrained model). Both plane-strain and plane-stress cases under tensile loading are considered. The perturbation analyses show that these boundary conditions are indeed closely related to the observed PLC band patterns.
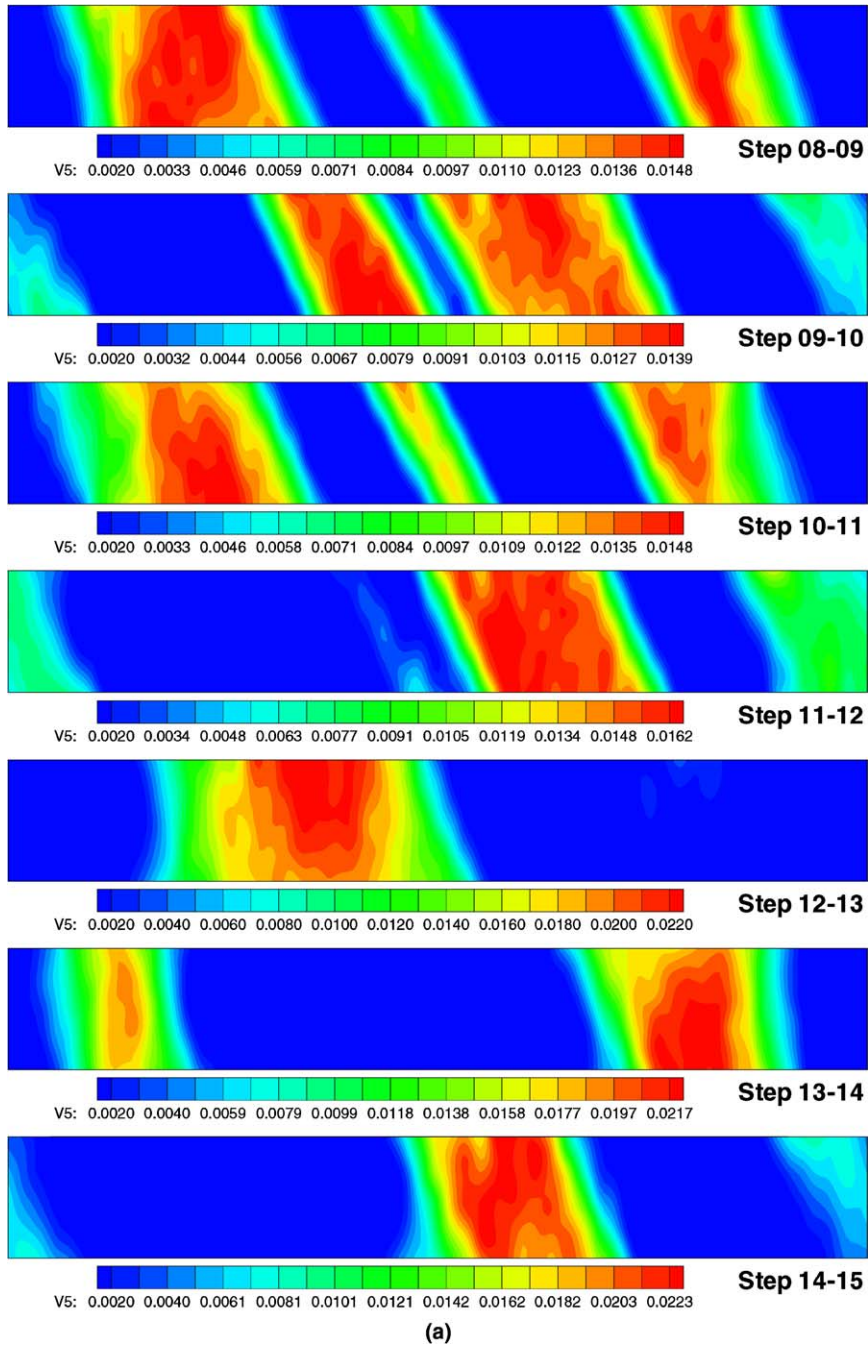
Fig. 1. Tensile incremental axial strain mapping results for AA6111-T4 sheet metal (Li, 2001): (a) the initial uncorrelated stage (inclined and multiple PLC bands); (b) the transition stage; (c) the correlated stage.
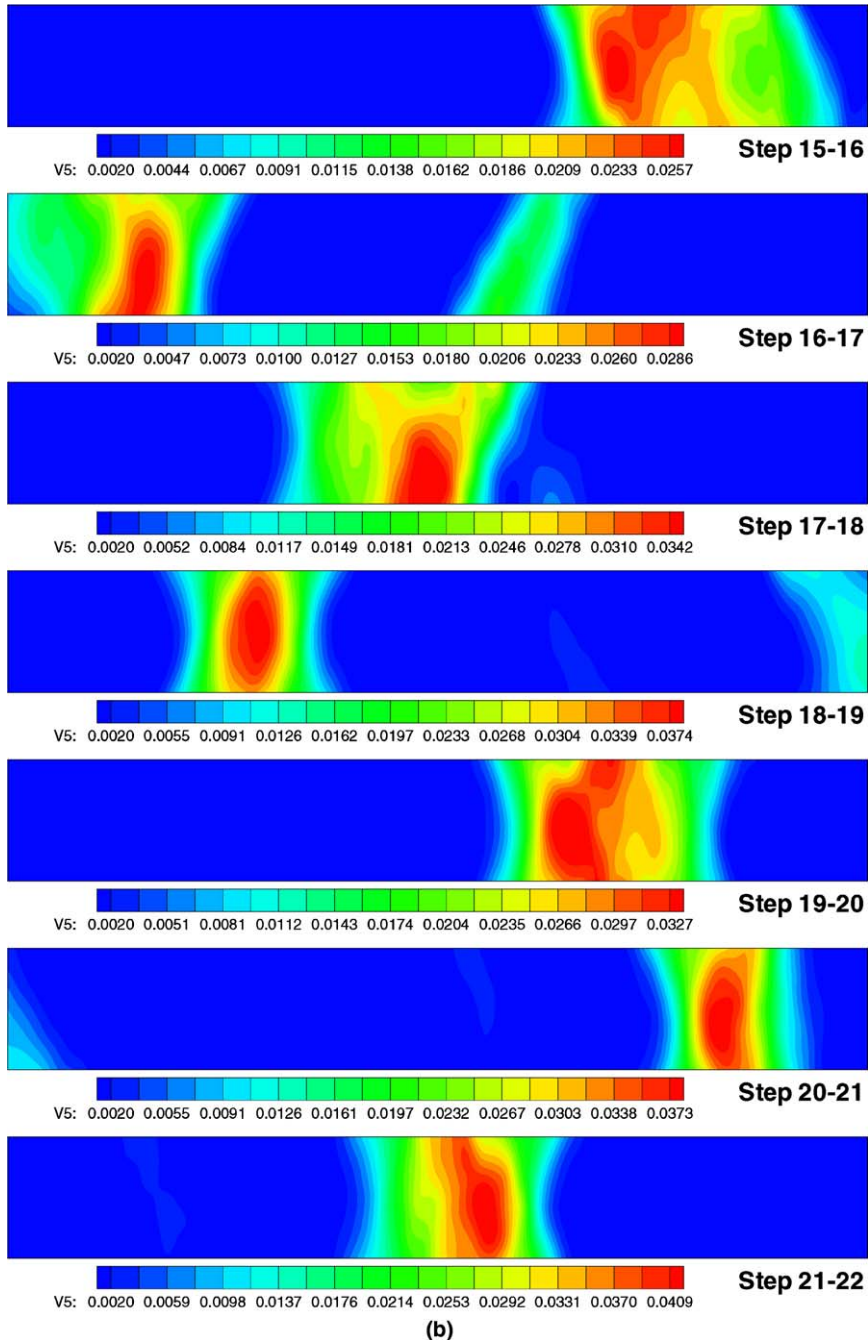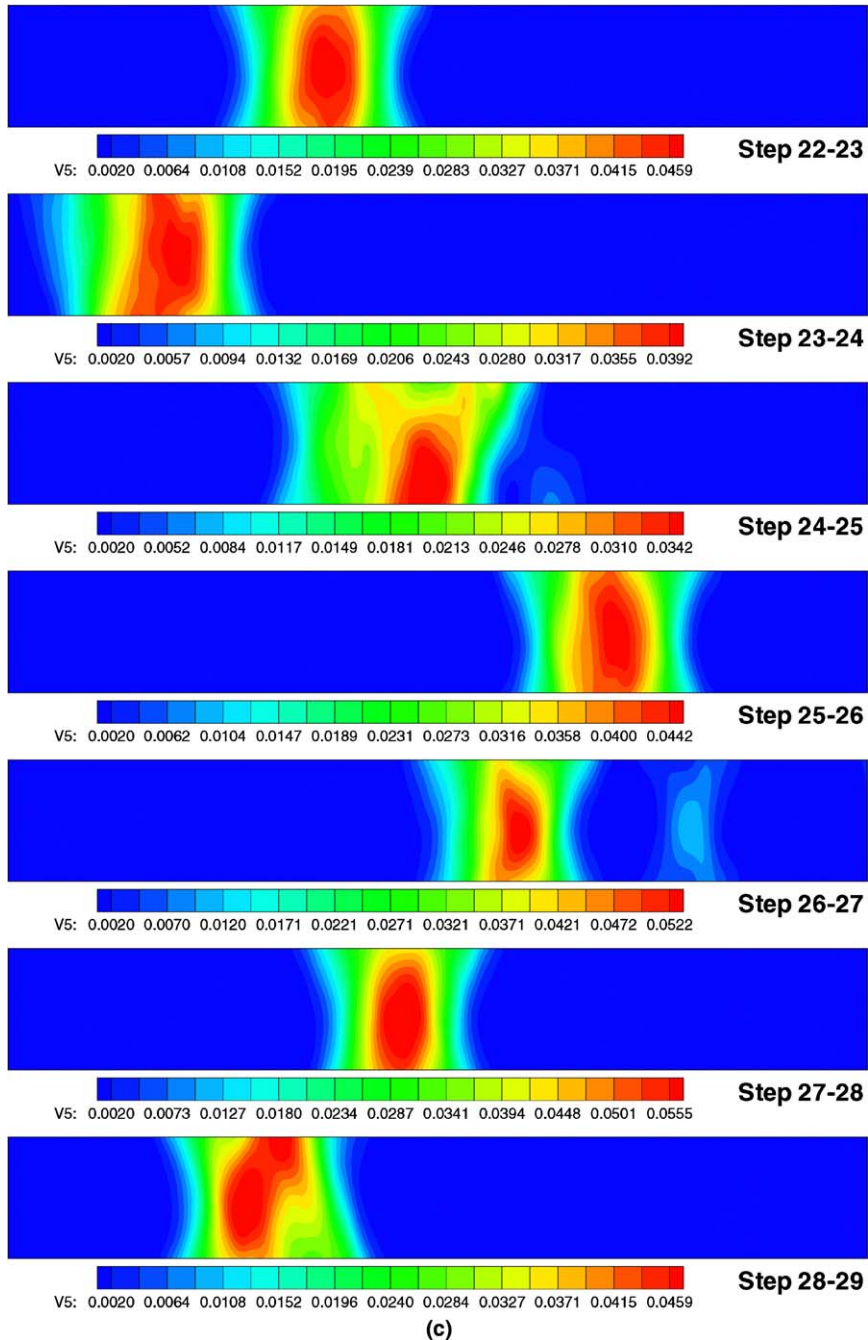
Fig. 1 (*continued*)

Fig. 1 (*continued*)

2. Governing equations

In this section, we describe the kinematics, constitutive formulations, and equilibrium equations for metal alloys undergoing dynamic strain aging using a framework of rate-dependent plasticity. The velocity gradient $\mathbf{L}$ for elasto-plastic deformations can be written as the sum of the symmetric rate of deformation $\mathbf{D}$ and anti-symmetric spin $\mathbf{W}$:

$$\mathbf{L} = \mathbf{D} + \mathbf{W}. \tag{1}$$

The rate of deformation and spin tensors can be decomposed into a lattice part (superscript *) and a plastic part (superscript p) as follows:

$$\mathbf{D} = \mathbf{D}^* + \mathbf{D}^p, \tag{2}$$

$$\mathbf{W} = \mathbf{W}^* + \mathbf{W}^p. \tag{3}$$

The elastic rate of deformation $\mathbf{D}^*$ is negligible in metals, and the plastic part of the above equations can be represented by shear strains associated with *slip modes*:

$$\mathbf{D} \approx \mathbf{D}^p = \sum_{\alpha=1}^{N} \dot{\gamma}_\alpha \mathbf{P}_\alpha, \tag{4}$$

$$\mathbf{W}^p = \sum_{\alpha=1}^{N} \dot{\gamma}_\alpha Q_\alpha, \tag{5}$$

where $\dot{\gamma}_\alpha$ is the rate of change of integrated shear strain for the αth slip mode, and N is the total number of the slip modes. We consider polycrystalline metals, and the slip modes refer to macroscopic slip systems averaged from the crystallographic slip systems of a set of grains (see Fig. 2). Ideally, there would be a very large number of the microscopic slip modes in polycrystalline samples. Analogous to the microscopic slips in grains in which only a few of them are activated and predominate, a small number of the effective macroscopic slip modes that meet the necessary kinematics compatibility requirements would be sufficient to describe the dominant plastic flow process in a polycrystalline aggregate. Dudzinski and Molinary (1991) used a conventional theory of plasticity in their perturbation analysis. The plastic flow surface in such a conventional theory may be too smooth and the polycrystalline samples may be treated to be too homogeneous to study the mechanisms of the band patterns observed in experiments. For example, when uniaxial tensile loading is applied, inclined shear band to the loading axis cannot be generated by the conventional flow rules.
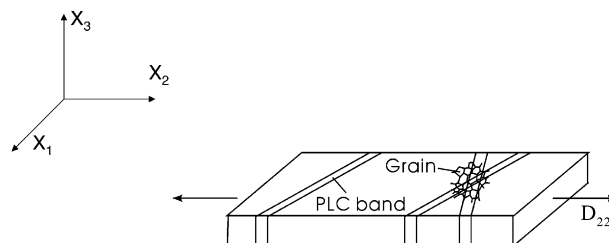

Fig. 2. Single and double PLC bands in a sheet metal. In plane-strain case, x_1, x_2, and x_3 directions correspond respectively to normal, rolling, and transverse directions. In plane-stress case, x_1, x_2, and x_3 directions correspond respectively to transverse, rolling, and normal directions.

A slip mode is composed of a slip direction and a slip plane. The Schmid factor $\mathbf{P}_\alpha$ and tensor $\mathbf{Q}_\alpha$ for the αth slip mode are defined respectively by

$$\mathbf{P}_\alpha = \mathrm{sym}\,\mathbf{T}_\alpha = \frac{1}{2}(\mathbf{s}_\alpha \otimes \mathbf{m}_\alpha + m_\alpha \otimes \mathbf{s}_\alpha), \tag{6}$$

$$\mathbf{Q}_\alpha = \mathrm{skew}\,\mathbf{T}_\alpha = \frac{1}{2}(\mathbf{s}_\alpha \otimes \mathbf{m}_\alpha - \mathbf{m}_\alpha \otimes \mathbf{s}_\alpha), \tag{7}$$

where tensor $\mathbf{T}_\alpha$ is defined by $\mathbf{T}_\alpha = \mathbf{s}_\alpha \otimes \mathbf{m}_\alpha$, and unit vectors $\mathbf{s}_\alpha$ and $\mathbf{m}_\alpha$ are the slip direction and normal to the slip plane associated with the αth slip mode in the deformed configuration, respectively.

In our rate-dependent viscoplasticity formulation, the cumulative slipping rate defined by $\dot{\bar{\gamma}}_\alpha = \mathrm{sign}(\dot{\gamma}_\alpha)\dot{\gamma}_\alpha$ is related to the resolved shear stress τ_α as follows (when τ_α is equal to or higher than a critical stress level or yield stress on each slip mode):

$$\dot{\bar{\gamma}}_\alpha = \dot{a}\left(\frac{\tau_\alpha}{g_\alpha}\right)^{\frac{1}{m}}\mathrm{e}^{-\beta C_{s\alpha}} \tag{8}$$

where m is the rate sensitivity exponent (whose value is assumed to make $1/m$ an even number for simplifying the analysis in the following), $\dot{a}$ is the reference strain rate, g_α is the yield strength, $C_{s\alpha}$ is solute concentration on the slip mode α, and β is a material constant (Yang and Tong, 2001). The resolved shear stresses τ_α on the slip planes in the current configuration are obtained by $\tau_\alpha = \mathbf{P}_\alpha : \boldsymbol{\sigma}$ where $\boldsymbol{\sigma}$ is the Cauchy stress. The strain hardening is characterized by the following expression:

$$\dot{g}_\alpha = h_\alpha \dot{\bar{\gamma}}_\alpha. \tag{9}$$

The hardening modulus h_α is taken to be

$$h_\alpha = h_0 \,\mathrm{sech}^2\left(\frac{h_0 \bar{\gamma}_\alpha}{\tau_s - \tau_0^\alpha}\right) \cdot \left(1 + \sum_{\beta \neq \alpha} f_{\alpha\beta} \tanh\frac{\bar{\gamma}_\beta}{\gamma_0}\right) \tag{10}$$

where h_0 is the initial hardening modulus, τ_0^α is the initial yield strength, τ_s is the saturation yield strength, γ_0 is the amount of slip after which the interaction between slip modes reach the peak strength, and $f_{\alpha\beta}$ represents the magnitude of interaction strength among slip modes in a polycrystalline solid. These material constants for each slip mode are polycrystalline quantities averaged from a collection of grains. Regarding the value of $f_{\alpha\beta}$, if a set of grains deforms along a particular slip mode as shown in Fig. 3, and the interaction between other sets of grains can be neglected, and then the polycrystalline latent hardening would be zero.
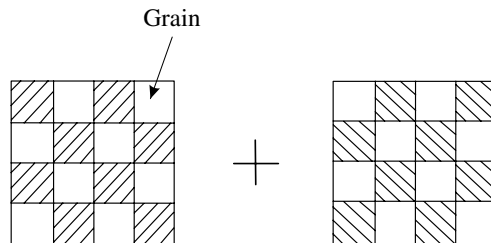

Fig. 3. Two set of grains deforming along two slip modes. Inclined lines represent slip lines. In this ideal case, the grains do not interact to each other, so the polycrystalline latent-hardening modulus will be equal to zero.

The static equilibrium equation is written as

$$\sum_{j=1}^{3} \frac{\partial \sigma_{ij}}{\partial x_j} = 0, \tag{11}$$

where body force is neglected.

3. Homogeneous solution in plane-strain case

A three-dimensional tensile specimen with rectangular cross-section cut from a polycrystalline sheet is shown in Fig. 2. We first consider plane-strain condition along the x_3 axis (transverse direction). The uniaxial tensile loading is applied along the x_2 axis (rolling direction). It is assumed that the normal vector to the slip modes stays on the plane normal to the x_3 axis, and the deformation is described by the in-plane shear strains on the slip modes by neglecting the out-of-plane deformation along the transverse direction. These assumptions satisfy the plane-strain condition, $D_{i3} = D_{3i} = 0$.

For uniaxial tensile loading along the x_2 axis, a duplex slip mode is assumed as shown in Fig. 4(a), and the slip modes are designated as slip modes one and two, respectively. The slip direction and normal to the slip planes are written in the laboratory coordinate system as:

$$\mathbf{s}_1 = (\sin \psi, \cos \psi, 0),$$
$$\mathbf{m}_1 = (-\cos \psi, \sin \psi, 0), \tag{12}$$

$$\mathbf{s}_2 = (-\sin (2\phi - \psi), \cos (2\phi - \psi), 0),$$
$$\mathbf{m}_2 = (\cos (2\phi - \psi), \sin (2\phi - \psi), 0). \tag{13}$$

The angle between the slip modes, ϕ, would depend on the texture of polycrystalline specimen. The angle ψ represents the angle between a slip mode and the x_2 axis. The angle ψ depends on the anisotropy of the specimen and the amount of the rigid body rotation. We will neglect texture development by deformation. The stress tensor can be written in the laboratory coordinate system as

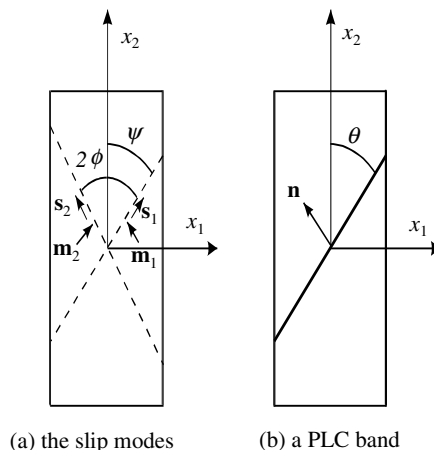(a) the slip modes   (b) a PLC band

Fig. 4. (a) Orientations of planar slip modes. Slip planes are denoted by the dotted lines. (b) Orientation of a PLC band.

$$\sigma = \begin{pmatrix} \sigma_{11} & \sigma_{12} & \sigma_{13} \\ \sigma_{12} & \sigma_{22} & \sigma_{23} \\ \sigma_{13} & \sigma_{23} & \sigma_{33} \end{pmatrix},$$

and the resolved shear stresses turn out to be

$$\tau_1 = \frac{1}{2}(\sigma_{22} - \sigma_{11})\sin 2\psi - \sigma_{12}\cos 2\psi, \tag{14}$$

$$\tau_2 = \frac{1}{2}(\sigma_{22} - \sigma_{11})\sin(4\phi - 2\psi) + \sigma_{12}\cos(4\phi - 2\psi). \tag{15}$$

Since the specimen is a thin sheet along the x_1 direction (normal direction), the values of σ_{11} and σ_{12} are small. The value of σ_{12} will be calculated in the numerical analysis. Using the equation in (4), the rate of deformation tensor is given by

$$\mathbf{D} = \begin{pmatrix} D_{11} & D_{12} & 0 \\ D_{12} & D_{22} & 0 \\ 0 & 0 & 0 \end{pmatrix},$$

where

$$D_{11} = -\frac{1}{2}\dot{\gamma}_1\sin 2\psi - \frac{1}{2}\dot{\gamma}_2\sin(4\phi - 2\psi), \tag{16}$$

$$D_{12} = -\frac{1}{2}\dot{\gamma}_1\cos 2\psi + \frac{1}{2}\dot{\gamma}_2\cos(4\phi - 2\psi), \tag{17}$$

$$D_{22} = \frac{1}{2}\dot{\gamma}_1\sin 2\psi + \frac{1}{2}\dot{\gamma}_2\sin(4\phi - 2\psi). \tag{18}$$

The value of D_{12} would be also small in (17) if $\dot{\gamma}_1 \approx \dot{\gamma}_2$ and $\phi \approx \psi$. The value will be checked in the analysis. The rate of rotation is given by the sum of the rigid body rotation and plastic parts:

$$W_{12} = \dot{\psi} + \frac{1}{2}(\dot{\gamma}_1 - \dot{\gamma}_2). \tag{19}$$

When a tensile loading is imposed in the x_2 direction, D_{22} is positive, and the resolved shear stresses and slipping rates are positive. One can obtain the expressions for the stresses from (8), (14) and (15):

$$\sigma_{22} - \sigma_{11} = \frac{2}{\sin 4\phi}\left(g_1\left(\frac{\dot{\gamma}_1}{\dot{a}}\right)^m e^{m\beta C_{s1}}\cos(4\phi - 2\psi) + g_2\left(\frac{\dot{\gamma}_2}{\dot{a}}\right)^m e^{m\beta C_{s2}}\cos 2\psi\right), \tag{20}$$

$$\sigma_{12} = \frac{1}{\sin 4\phi}\left(-g_1\left(\frac{\dot{\gamma}_1}{\dot{a}}\right)^m e^{m\beta C_{s1}}\sin(4\phi - 2\psi) + g_2\left(\frac{\dot{\gamma}_2}{\dot{a}}\right)^m e^{m\beta C_{s2}}\sin 2\psi\right). \tag{21}$$

At the initial stage of the tensile loading of polycrystalline metals, the compatibility condition between neighboring grains would be negligible, and each grain of the single crystal is subject to the same homogeneous stress as being assumed in the Sachs model of the polycrystal aggregate (Khan and Huang, 1995). Hence shear stress σ_{12} is assumed to vanish, and we will call this the unconstrained model. Using the condition of $\sigma_{12} = 0$, one can obtain the expressions for the slipping rates and tensile stress during the deformation from (18), (20) and (21):

$$\dot{\bar{\gamma}}_2 = \left(\frac{g_1 e^{m\beta C_{s1}} \sin(4\phi - 2\psi)}{g_2 e^{m\beta C_{s2}} \sin 2\psi}\right)^{\frac{1}{m}} \dot{\bar{\gamma}}_1, \tag{22}$$

$$\dot{\bar{\gamma}}_1 = \frac{2D_{22}(g_2 e^{m\beta C_{s2}} \sin 2\psi)^{\frac{1}{m}}}{g_1^{1/m} e^{\beta C_{s1}} (\sin(4\phi - 2\psi))^{1+1/m} + g_2^{1/m} e^{\beta C_{s2}} (\sin 2\psi)^{1+1/m}}, \tag{23}$$

$$\sigma_{22} - \sigma_{11} = \frac{2g_1 g_2 e^{m\beta C_{s1}} e^{m\beta C_{s2}}}{\left(g_1^{1/m} e^{\beta C_{s1}} (\sin(4\phi - 2\psi))^{1+1/m} + g_2^{1/m} e^{\beta C_{s2}} (\sin 2\psi)^{1+1/m}\right)^m} \left(\frac{2D_{22}}{\dot{a}}\right)^m. \tag{24}$$

On the other hand, at the later stage of the tensile loading, the yield strength is spatially homogeneous, and the hardening modulus becomes small. Each grain of the single crystal can be thought of as being subjected to the same homogeneous deformation as being assumed in the Taylor model of the polycrystal aggregate (Khan and Huang, 1995). Hence shear component D_{12} of the rate of deformation tensor is assumed to vanish, and we will call this the constrained model. Using the condition of $D_{12} = 0$, one can get the expressions for the cumulative slipping rates as follow:

$$\dot{\bar{\gamma}}_2 = \left|\frac{\cos 2\psi}{\cos(4\phi - 2\psi)}\right| \dot{\bar{\gamma}}_1, \quad \text{for } 2\phi - \psi \neq \frac{\pi}{4}, \tag{25}$$

$$\dot{\bar{\gamma}}_1 = 2D_{22} \left|\frac{\cos(4\phi - 2\psi)}{\sin 4\phi}\right|, \quad \text{for } \phi \neq \frac{\pi}{4}. \tag{26}$$

If $\phi = \psi = \pi/4$, one should use $\dot{\bar{\gamma}}_2 = \dot{\bar{\gamma}}_1$ and $\dot{\bar{\gamma}}_1 = D_{22}$ instead of (25) and (26). Using (20), (21), (25) and (26), one can get the expressions for the stress components for $\phi \neq \pi/4$:

$$\sigma_{22} - \sigma_{11} = \frac{2g_1 e^{m\beta C_{s1}} \cos(4\phi - 2\psi) |\cos(4\phi - 2\psi)|^m + 2g_2 e^{m\beta C_{s2}} \cos 2\psi |\cos 2\psi|^m}{\sin 4\phi |\sin 4\phi|^m} \left(\frac{2D_{22}}{\dot{a}}\right)^m, \tag{27}$$

$$\sigma_{12} = \frac{-g_1 e^{m\beta C_{s1}} \sin(4\phi - 2\psi) |\cos(4\phi - 2\psi)|^m + g_2 e^{m\beta C_{s2}} \sin 2\psi |\cos 2\psi|^m}{\sin 4\phi |\sin 4\phi|^m} \left(\frac{2D_{22}}{\dot{a}}\right)^m. \tag{28}$$

The unknowns are $\bar{\gamma}_1$, $\bar{\gamma}_2$, g_1, g_2, $(\sigma_{22} - \sigma_{11})$, σ_{12}, V_1, V_2, ψ, C_{s1}, C_{s2}, t_{w1}, t_{w2}, γ_1 and γ_2. The following 15 governing equations relate these 15 unknowns. Combining (8), (14) and (15), one can obtain the relations between the cumulative slipping rates and the stresses for the case of positive resolved shear stresses:

$$g_1 e^{m\beta C_{s1}} \left(\frac{\dot{\bar{\gamma}}_1}{\dot{a}}\right)^m = \frac{1}{2}(\sigma_{22} - \sigma_{11}) \sin 2\psi - \sigma_{12} \cos 2\psi, \tag{29}$$

$$g_2 e^{m\beta C_{s2}} \left(\frac{\dot{\bar{\gamma}}_2}{\dot{a}}\right)^m = \frac{1}{2}(\sigma_{22} - \sigma_{11}) \sin(4\phi - 2\psi) + \sigma_{12} \cos(4\phi - 2\psi). \tag{30}$$

The yield strengths are obtained by integrating the hardening equations as follows:

$$\dot{g}_1 = h_1 \dot{\bar{\gamma}}_1, \tag{31}$$
$$\dot{g}_2 = h_2 \dot{\bar{\gamma}}_2. \tag{32}$$

The rate of rotation in (19) is expressed as

$$\frac{\partial V_1}{\partial x_2} - \frac{\partial V_2}{\partial x_1} = 2\dot{\psi} + (\dot{\gamma}_1 - \dot{\gamma}_2). \tag{33}$$

By differentiating the equilibrium equations in (11), and subtracting them, one can obtain

$$\frac{\partial^2}{\partial x_1 \partial x_2}(\sigma_{22} - \sigma_{11}) + \left(\frac{\partial^2}{\partial x_1^2} - \frac{\partial^2}{\partial x_2^2}\right)\sigma_{12} = 0. \tag{34}$$

The velocities are related to the slipping rates by (16) and (17):

$$\frac{\partial V_1}{\partial x_1} = -\frac{1}{2}\dot{\gamma}_1 \sin 2\psi - \frac{1}{2}\dot{\gamma}_2 \sin(4\phi - 2\psi), \tag{35}$$

$$\frac{\partial V_1}{\partial x_2} + \frac{\partial V_2}{\partial x_1} = -\dot{\gamma}_1 \cos 2\psi + \dot{\gamma}_2 \cos(4\phi - 2\psi). \tag{36}$$

From the property of volume preservation of slipping

$$\frac{\partial V_1}{\partial x_1} + \frac{\partial V_2}{\partial x_2} = 0. \tag{37}$$

The cumulative slipping rates are defined by

$$\dot{\bar{\gamma}}_1 = \text{sign}(\dot{\gamma}_1)\dot{\gamma}_1, \tag{38}$$

$$\dot{\bar{\gamma}}_2 = \text{sign}(\dot{\gamma}_2)\dot{\gamma}_2. \tag{39}$$

The concentration of solute atoms on each slip plane is defined by the following expression:

$$C_{s1} = C_m - C_m e^{-\left(\frac{t_{w1}}{\tau}\right)^{\frac{2}{3}}}, \tag{40}$$

$$C_{s2} = C_m - C_m e^{-\left(\frac{t_{w2}}{\tau}\right)^{\frac{2}{3}}}, \tag{41}$$

where C_m is the maximum solute concentration, and τ is a characteristic time. From the Orowan equation relating the plastic strain rate to the average velocity and the density of mobile dislocations, the waiting time for a dislocation to be unpinned is inversely proportional to the plastic strain rate

$$t_{w1} = \frac{C\bar{\gamma}_1}{\dot{\bar{\gamma}}_1}, \tag{42}$$

$$t_{w2} = \frac{C\bar{\gamma}_2}{\dot{\bar{\gamma}}_2}, \tag{43}$$

where $\bar{\gamma}_\alpha$ is the cumulative shear strain on the αth slip mode.

4. Homogeneous solution in plane-stress case

For the plane-stress condition along the x_3 axis in Fig. 4, the x_1 axis correspond to the transverse direction, and the out-of-plane components of the stress tensors are equal to zero ($\sigma_{i3} = \sigma_{3i} = 0$). It is assumed that the strain increments along the x_1 and x_3 axes are equal (Dieter, 1988)

$$D_{11} = D_{33} = -\frac{1}{2}D_{22}. \tag{44}$$

To obtain a plastic deformation rates satisfying equation in (44), we assume the following four slip modes:

$$\mathbf{s}_1 = (a, b, 0), \quad \mathbf{s}_2 = (-\bar{a}, \bar{b}, 0), \quad \mathbf{s}_3 = (0, a, b), \quad \mathbf{s}_4 = (0, -\bar{a}, \bar{b}),$$

$$\mathbf{m}_1 = (-b, a, 0), \quad \mathbf{m}_2 = (\bar{b}, \bar{a}, 0), \quad \mathbf{m}_3 = (0, -b, a), \quad \text{and} \quad \mathbf{m}_4 = (0, \bar{b}, \bar{a}),$$

where $a = \sin\psi$, $b = \cos\psi$, $\bar{a} = \sin(2\phi - \psi)$ and $\bar{b} = \cos(2\phi - \psi)$. If $\dot\gamma_3 = -\dot\gamma_1$ and $\dot\gamma_4 = -\dot\gamma_2$, the equation in (44) is satisfied. Then the velocity gradient is given by

$$\mathbf{L} = \dot\gamma_1(\mathbf{T}_1 - \mathbf{T}_2) + \dot\gamma_2(\mathbf{T}_3 - \mathbf{T}_4) + W^*, \quad \text{where } \mathbf{T}_\alpha = \mathbf{s}_\alpha \otimes m_\alpha.$$

The stress tensor is written as

$$\sigma = \begin{pmatrix} \sigma_{11} & \sigma_{12} & 0 \\ \sigma_{12} & \sigma_{22} & 0 \\ 0 & 0 & 0 \end{pmatrix},$$

and the resolved shear stresses on the slip modes are related to the stress tensor by

$$\tau_1 - \tau_3 = (\mathbf{P}_1 - \mathbf{P}_3) : \boldsymbol\sigma = \left(\sigma_{22} - \frac{1}{2}\sigma_{11}\right) \sin 2\psi - \sigma_{12} \cos 2\psi \tag{45}$$

$$\tau_2 - \tau_4 = (\mathbf{P}_2 - \mathbf{P}_4) : \boldsymbol\sigma = \left(\sigma_{22} - \frac{1}{2}\sigma_{11}\right) \sin(4\phi - 2\psi) + \sigma_{12} \cos(4\phi - 2\psi) \tag{46}$$

The values of σ_{11} and σ_{12} will be small in uniaxial tensile loading along the x_2 direction. Using the equation in (4), the rate of deformation tensor is given by

$$\mathbf{D} = \begin{pmatrix} D_{11} & D_{12} & D_{13} \\ D_{12} & D_{22} & D_{23} \\ D_{13} & D_{23} & D_{33} \end{pmatrix},$$

where

$$D_{11} = -\frac{1}{2}\dot\gamma_1 \sin 2\psi - \frac{1}{2}\dot\gamma_2 \sin(4\phi - 2\psi), \tag{47}$$

$$D_{22} = \dot\gamma_1 \sin 2\psi + \dot\gamma_2 \sin(4\phi - 2\psi), \tag{48}$$

$$D_{33} = D_{11}, \tag{49}$$

$$D_{12} = -\frac{1}{2}\dot\gamma_1 \cos 2\psi + \frac{1}{2}\dot\gamma_2 \cos(4\phi - 2\psi), \tag{50}$$

$$D_{23} = -D_{12}, \quad D_{13} = 0. \tag{51}$$

The shear components of the rate of deformation tensor will be small in (50) and (51).

The relation between the resolved shear stresses and slipping rates are written as

$$\tau_1 - \tau_3 = g_1 \left(\frac{\dot{\bar\gamma}_1}{\dot{a}}\right)^m e^{m\beta C_{s1}} + g_3 \left(\frac{\dot{\bar\gamma}_3}{\dot{a}}\right)^m e^{m\beta C_{s3}} = 2g_1 \left(\frac{\dot{\bar\gamma}_1}{\dot{a}}\right)^m e^{m\beta C_{s1}},$$

$$\tau_2 - \tau_4 = g_2 \left(\frac{\dot{\bar\gamma}_2}{\dot{a}}\right)^m e^{m\beta C_{s2}} + g_4 \left(\frac{\dot{\bar\gamma}_4}{\dot{a}}\right)^m e^{m\beta C_{s4}} = 2g_2 \left(\frac{\dot{\bar\gamma}_2}{\dot{a}}\right)^m e^{m\beta C_{s2}},$$

where $g_3 = g_1$, $g_4 = g_2$, $C_{s3} = C_{s1}$ and $C_{s4} = C_{s2}$ are used. Solving the above two equations for the stress components, one can obtain

$$\sigma_{22} - \frac{1}{2}\sigma_{11} = \frac{2}{\sin 4\phi} \left(g_1 \left(\frac{\dot{\bar\gamma}_1}{\dot{a}}\right)^m e^{m\beta C_{s1}} \cos(4\phi - 2\psi) + g_2 \left(\frac{\dot{\bar\gamma}_2}{\dot{a}}\right)^m e^{m\beta C_{s2}} \cos 2\psi\right),$$

$$\sigma_{12} = \frac{2}{\sin 4\phi} \left(-g_1 \left(\frac{\dot{\bar\gamma}_1}{\dot{a}}\right)^m e^{m\beta C_{s1}} \sin(4\phi - 2\psi) + g_2 \left(\frac{\dot{\bar\gamma}_2}{\dot{a}}\right)^m e^{m\beta C_{s2}} \sin 2\psi\right).$$

Following the same procedures as the plane-strain case for the unconstrained model, one can get the same relation between $\dot{\bar{\gamma}}_1$ and $\dot{\bar{\gamma}}_2$ as (22). The other equations for $\dot{\bar{\gamma}}_1$ and $\sigma_{22} - \frac{1}{2}\sigma_{11}$ are given by

$$\dot{\bar{\gamma}}_1 = \frac{D_{22}(g_2 \mathrm{e}^{m\beta C_{s2}} \sin 2\psi)^{\frac{1}{m}}}{g_1^{1/m} \mathrm{e}^{\beta C_{s1}} (\sin(4\phi - 2\psi))^{1+1/m} + g_2^{1/m} \mathrm{e}^{\beta C_{s2}} (\sin 2\psi)^{1+1/m}}, \tag{52}$$

$$\sigma_{22} - \frac{1}{2}\sigma_{11} = \frac{2g_1 g_2 \mathrm{e}^{m\beta C_{s1}} \mathrm{e}^{m\beta C_{s2}}}{\left(g_1^{1/m} \mathrm{e}^{\beta C_{s1}} (\sin(4\phi - 2\psi))^{1+1/m} + g_2^{1/m} \mathrm{e}^{\beta C_{s2}} (\sin 2\psi)^{1+1/m}\right)^m} \left(\frac{D_{22}}{\dot{a}}\right)^m. \tag{53}$$

Using the condition of $D_{12} = 0$ for the constrained model, one can get the same expression between $\dot{\bar{\gamma}}_1$ and $\dot{\bar{\gamma}}_2$ as (25) for $2\phi - \psi \neq \pi/4$. The other equations for $\dot{\bar{\gamma}}_1$, $\sigma_{22} - \frac{1}{2}\sigma_{11}$ and σ_{12} are given for $\phi \neq \pi/4$ by

$$\dot{\bar{\gamma}}_1 = D_{22} \left| \frac{\cos(4\phi - 2\psi)}{\sin 4\phi} \right|, \tag{54}$$

$$\sigma_{22} - \frac{1}{2}\sigma_{11} = \frac{2g_1 \mathrm{e}^{m\beta C_{s1}} \cos(4\phi - 2\psi)|\cos(4\phi - 2\psi)|^m + 2g_2 \mathrm{e}^{m\beta C_{s2}} \cos 2\psi |\cos 2\psi|^m}{\sin 4\phi |\sin 4\phi|^m} \left(\frac{D_{22}}{\dot{a}}\right)^m, \tag{55}$$

$$\sigma_{12} = \frac{-2g_1 \mathrm{e}^{m\beta C_{s1}} \sin(4\phi - 2\psi)|\cos(4\phi - 2\psi)|^m + 2g_2 \mathrm{e}^{m\beta C_{s2}} \sin 2\psi |\cos 2\psi|^m}{\sin 4\phi |\sin 4\phi|^m} \left(\frac{D_{22}}{\dot{a}}\right)^m. \tag{56}$$

The unknowns are $\bar{\gamma}_1$, $\bar{\gamma}_2$, g_1, g_2, $(\sigma_{22} - \frac{1}{2}\sigma_{11})$, σ_{12}, V_1, V_2, ψ, C_{s1}, C_{s2}, t_{w1}, t_{w2}, γ_1, and γ_2, and the same procedures as for Eqs. (29)–(43) are followed to derive the corresponding equations for the homogeneous solutions in the plane-stress case.

5. Perturbed analysis

For a tensile specimen, there are several criteria for the onset of strain localization. In the classical approach, the conditions of diffuse necking and localized necking can be considered (Dieter, 1988). For both of them, localized deformation begins where the increase in stress due to the decrease in the cross-sectional area of the specimen becomes greater than the increase of the yield strength due to strain hardening. If the specimen is a sheet metal, then localized necking follows diffuse necking. In the localized necking mode, the neck is a narrow shear band inclined at an angle to the specimen axis, and the length of the shear band remains constant. On the other hand, in bifurcation analysis, the difference in the velocity gradient inside and outside the shear band is considered, and the critical strain-hardening rate at the onset of localized deformation is obtained. (Bassani, 1994; Dao and Asaro, 1996). In this paper, the polycrystalline material undergoes dynamic strain aging, and we are interested in explaining the localized deformation patterns associated with dynamic strain aging using perturbation analysis. Our perturbation formulation is based on a model developed by Zikry et al. (2000).

In perturbation analysis, the stability of the material is analyzed by adding a small change to the homogeneous solution. The growth or decay of this small change with time characterizes the stability. The form of the perturbed solution, S_i, is given by (Zikry et al., 2000)

$$S_i = S_i^0 + \delta S_i = S_i^0 + \varepsilon S_i^* \mathrm{e}^{\eta(t-t_0)} \cos(\xi \mathbf{n} \cdot \mathbf{x}) \tag{57}$$

where the superscript 0 denotes the homogeneous solution, δS_i is the perturbation, ε is a small number, S_i^* is the initial value at time t_0, and ξ is the wave number. Unit vector $\mathbf{n}$ is defined by $\mathbf{n} = (-\cos\theta, \sin\theta)$, where θ determines the orientation of the PLC band with respect to the x_2 direction (see Fig. 4(b)). For the velocity components, the following form is used:

$$V_i = V_i^0 + \varepsilon V_i^* e^{\eta(t-t_0)} \sin(\xi \mathbf{n} \cdot \mathbf{x}). \tag{58}$$

If the real part of η, the perturbation growth rate, is positive, the perturbation will grow. Retaining the zeroth and first-order terms in the perturbed equations, the zeroth order terms correspond to the homogeneous solutions, and the first-order terms result in a linear system of equations of the form

$$\sum_j A_{ij} S_j^* = 0. \tag{59}$$

The equations in (59) can be written as the following matrix form:

$$
\begin{pmatrix}
A_{1,1} & 0 & A_{1,3} & 0 & A_{1,5} & A_{1,6} & 0 & 0 & A_{1,9} & A_{1,10} & 0 & 0 & 0 & 0 & 0 \\
0 & A_{2,2} & 0 & A_{2,4} & A_{2,5} & A_{2,6} & 0 & 0 & A_{2,9} & 0 & A_{2,11} & 0 & 0 & 0 & 0 \\
h_1 & 0 & -1 & 0 & 0 & 0 & 0 & 0 & 0 & 0 & 0 & 0 & 0 & 0 & 0 \\
0 & h_2 & 0 & -1 & 0 & 0 & 0 & 0 & 0 & 0 & 0 & 0 & 0 & 0 & 0 \\
0 & 0 & 0 & 0 & 0 & 0 & -n_2\xi & n_1\xi & A_{5,9} & 0 & 0 & 0 & 0 & A_{5,14} & A_{5,15} \\
0 & 0 & 0 & 0 & A_{6,5} & A_{6,6} & 0 & 0 & 0 & 0 & 0 & 0 & 0 & 0 & 0 \\
0 & 0 & 0 & 0 & 0 & 0 & A_{7,7} & 0 & A_{7,9} & 0 & 0 & 0 & 0 & A_{7,14} & A_{7,15} \\
0 & 0 & 0 & 0 & 0 & 0 & A_{8,7} & A_{8,8} & A_{8,9} & 0 & 0 & 0 & 0 & A_{8,14} & A_{8,15} \\
0 & 0 & 0 & 0 & 0 & 0 & A_{9,7} & n_2\xi & 0 & 0 & 0 & 0 & 0 & 0 & 0 \\
1 & 0 & 0 & 0 & 0 & 0 & 0 & 0 & 0 & 0 & 0 & 0 & 0 & A_{10,14} & 0 \\
0 & 1 & 0 & 0 & 0 & 0 & 0 & 0 & 0 & 0 & 0 & 0 & 0 & 0 & A_{11,15} \\
0 & 0 & 0 & 0 & 0 & 0 & 0 & 0 & 0 & 1 & 0 & A_{12,12} & 0 & 0 & 0 \\
0 & 0 & 0 & 0 & 0 & 0 & 0 & 0 & 0 & 0 & 1 & 0 & A_{13,13} & 0 & 0 \\
A_{14,1} & 0 & 0 & 0 & 0 & 0 & 0 & 0 & 0 & 0 & 0 & -1 & 0 & 0 & 0 \\
0 & A_{15,2} & 0 & 0 & 0 & 0 & 0 & 0 & 0 & 0 & 0 & 0 & -1 & 0 & 0
\end{pmatrix}
\times
\begin{pmatrix}
\bar{\gamma}_1^* \\
\bar{\gamma}_2^* \\
g_1^* \\
g_2^* \\
(\sigma_{22} - r\sigma_{11})^* \\
\sigma_{12}^* \\
V_1^* \\
V_2^* \\
\psi^* \\
C_{s1}^* \\
C_{s2}^* \\
t_{w1}^* \\
t_{w2}^* \\
\gamma_1^* \\
\gamma_2^*
\end{pmatrix}
= \mathbf{0}. \tag{60}
$$

The value of r is equal to 1 for the plane-strain case and 1/2 for the plane-stress case. The components of the coefficient matrix are listed in Appendix A. Non-trivial solutions exist only if

$$\det \left(A_{ij} \right) = 0. \tag{61}$$

The above equation is solved for η. The roots will change during deformation because the coefficient matrix depends on the homogeneous solutions such as the stress, shear strains, yield strengths, solute concentrations, waiting times, and orientation of slip modes, which change with time. In our numerical analysis those quantities are updated with time to find the rate of perturbation growth, Re(η), at the current time. That is, for the plane-strain case, the shear strains are updated by the one-step Euler's method after obtaining slipping rates from (22) and (23) or (25) and (26) for a given value of D_{22}, and the yield strengths g_1^0 and g_2^0 are updated at each time step by using (31) and (32). The solute concentrations and waiting times are determined by (40)–(43). One of the roots of η whose real part is both positive and also higher than the others is considered to study the localization behavior.

6. Numerical results

In an experimental work on plane-strain compression of polycrystals of an aluminum alloy (Harren et al., 1988), the angle between the traces of macroscopic shear bands and the elongation axis varied between 20° and 70° with an average value around 35–40°. In Li's experiments on simple tension of sheet polycrystalline aluminum alloys (Li, 2001), the angle between the PLC bands and the elongation axis was about 60°. At the early stage of the deformation, the increment of elongation strain during a time interval was oblique to the tensile axis. At the later stage, double bands developed, and the strain increment was seemingly perpendicular to the tensile axis.

In simple tension, the maximum shear stress is along ±45° to the tensile axis, and the most active slip mode would be along the same direction if the polycrystalline material is isotropic without any texture. In this paper, uniaxial loading is considered, and the slip modes are assumed to be symmetric to the tensile axis, and the rigid body rotation is neglected ($\dot{\psi}^0 = 0$). The value of 44° instead of 45° has been tried as the

Table 1
Numerical parameters

| Parameter	Value
Initial hardening modulus, h_0 (MPa)	1000
Initial yield strength of slip mode 1, τ_0^1 (MPa)	100
Initial yield strength of slip mode 2, τ_0^2	$1.0001\tau_0^1 \cdot 1.001\tau_0^1$ in Fig. 9
Saturation yield strength, τ_s (MPa)	300
Reference slip amount, γ_0	0.001
Slip interaction, f_{12}	5
Rate sensitivity exponent, m	0.02
Reference strain rate, $\dot{a}(\text{s}^{-1})$	0.001
Angle of slip modes, ϕ	44°
Angle of slip mode, ψ	44°
Material constant, β	800
Characteristic time, τ (s)	22.51
Maximum solute concentration, C_m	0.01
Material constant, C	0.015
Wave number, ξ (m)	100
Strain rate, D_{22} (s^{-1})	0.0001
Time increment, Δt (s)	20
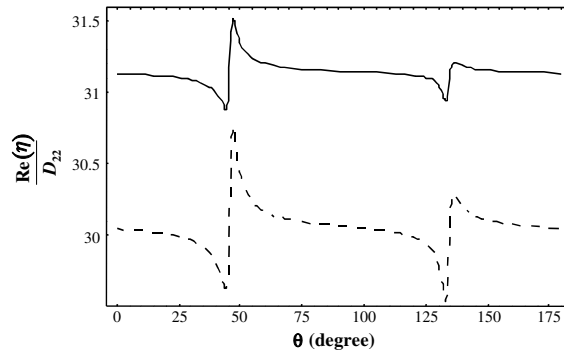
Fig. 5. Perturbation growth parameters at two different times in unconstrained model. Plane-strain case is considered. Solid line is at $\varepsilon_{22} = 0.058$, and dashed line at $\varepsilon_{22} = 0.06$. PLC band develops along two directions alternatively with time. The angle between PLC bands and the tensile axis is about 45°.
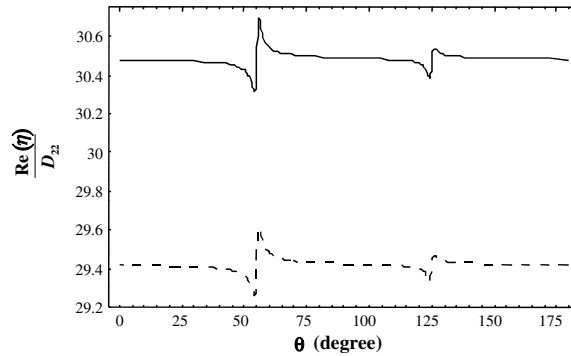

Fig. 6. Perturbation growth parameters at two different times in unconstrained model. Plane-stress case is considered. Solid line is at $\varepsilon_{22} = 0.052$, and dashed line at $\varepsilon_{22} = 0.054$. PLC band develops along two directions alternatively with time. The angle between PLC bands and the tensile axis is about 60°, which is larger than in plane-strain case.
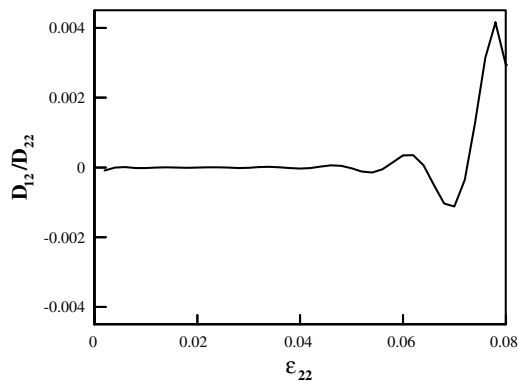

Fig. 7. Shear rate of deformation with respect to tensile strain in plane-strain case. Shear rate of deformation is very small compared to tensile rate of deformation, and the value oscillates around zero.

value of the symmetry angle ϕ; in the case of 45°, there is no qualitative difference from the case of 44°, except that sharper peaks are obtained at the angle of shear band. The values of the symmetry angle, ϕ, keep fixed through the whole deformation, assuming that there is no texture development by deformation. Nonsymmetrical initial yield strengths were introduced by $\tau_0^2 = 1.0001\tau_0^1$ or $\tau_0^2 = 1.001\tau_0^1$ to account for material inhomogeneities initially existing in the real specimens. The wave number ξ is related to the inverse of the size of the imperfection, and the value is taken to be 100 (Zikry et al., 2000). The other numerical parameters are listed in Table 1.

In the case of the unconstrained model, the tensile stress $(\sigma_{22} - \sigma_{11})^0$ was obtained by (24) for the plane-strain case, and $(\sigma_{22} - \sigma_{11}/2)^0$ by (53) for the plane-stress case. The shear stress σ_{12}^0 is equal to zero. The most positive perturbation growth parameter among the three roots of η is plotted with respect to the orientation of the PLC band, θ, in Figs. 5 and 6. The instability is caused by dynamic strain aging; in simple materials without dynamic strain aging, the perturbation growth rate turned out to be negative for sufficient strain-hardening. The maximum perturbation growth rate appears at one angle at a time, which means deformation becomes localized along one direction at a time. The numerical results are in agreement with the experimental observations. In the numerical analysis, after the material is strain-hardened, the PLC band flips to the other direction. By comparing Figs. 5 and 6, the angle of the PLC bands to the tensile axis is about 55° in the case of plane-stress, which is a little larger than 45° in plane-strain case. The
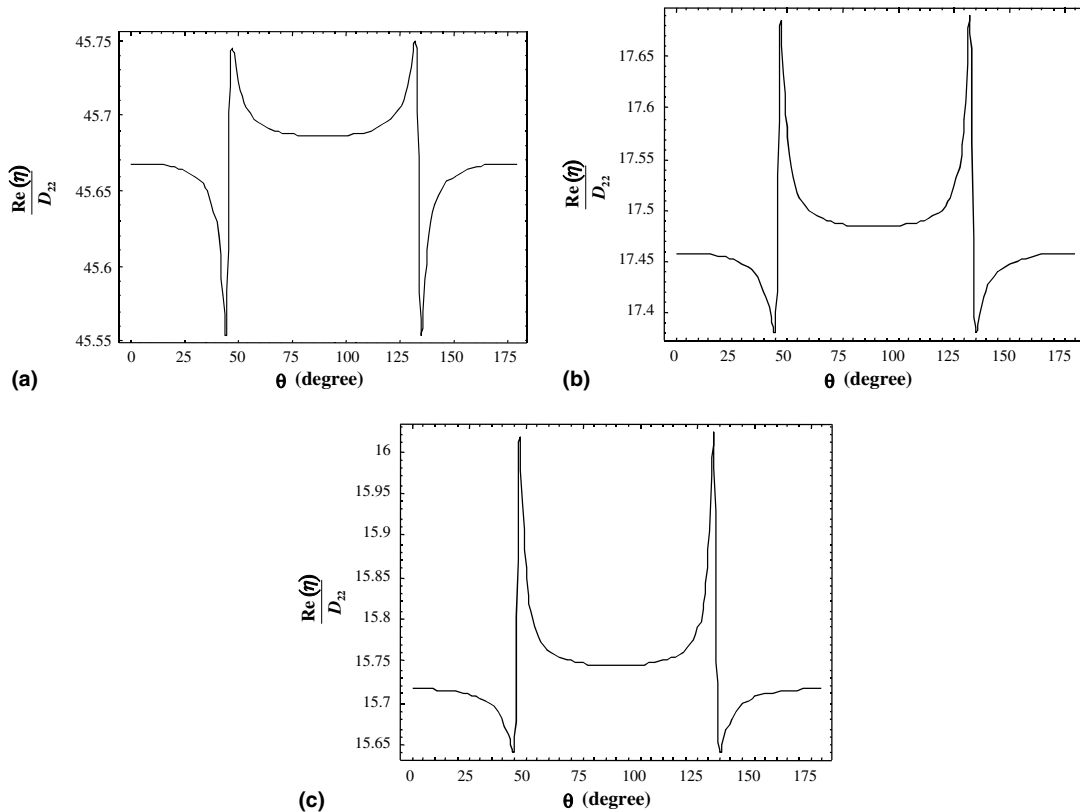

Fig. 8. Perturbation growth parameter at three different times in constrained model. Plane-strain case is considered. Initial material inhomogeneity is assumed by $\tau_0^2 = 1.0001\tau_0^1$. PLC bands develop along two directions simultaneously. The angle between PLC bands and the tensile axis is about 45°.
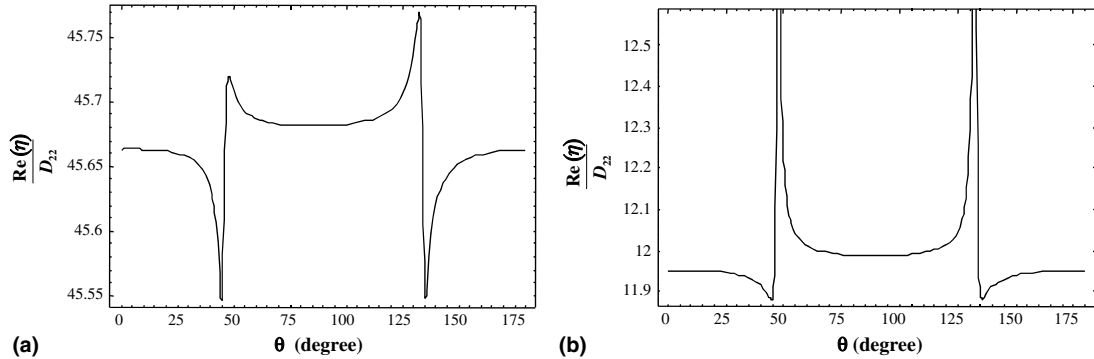
Fig. 9. Perturbation growth parameter at two different times in constrained model. Plane-strain case is considered. Initial material inhomogeneity is assumed by $\tau_0^2 = 1.001\tau_0^1$. A single PLC band appears at small strain, and double bands develop along two directions simultaneously at large strain. The angle between PLC bands and the tensile axis is about 45°.

experimental value for the angle of the PLC band in plane-stress case is about 60°, which is little bit larger than 55°. This difference may be caused by the assumption of the same strain rate along the normal and transverse directions. In experiment, the ratio of strains was between 0.5 and 0.7: that is, the contraction along the normal direction was larger than along the transverse direction. Fig. 7 shows the value of D_{12} with respect to the tensile strain in the plane-strain case. One can confirm that the value of D_{12} is very small compared to D_{22}.

In the case of the constrained model, the shear component D_{12} of the rate of deformation is assumed to be zero, and the stresses were obtained by (27) and (28) for plane-strain case, and by (55) and (56) for plane-stress case. The perturbation growth rates at different times are shown in Figs. 8–10. In this case, if the initial material inhomogeneity is small ($\tau_0^2 = 1.0001\tau_0^1$), the growth rate has the same positive maximum levels at two symmetric angles, which means that symmetric double bands develop. If the initial material inhomogeneity is large ($\tau_0^2 = 1.001\tau_0^1$), then a single band appears at small strain, and double bands are observed at large strain (see Fig. 9). These numerical results are in agreement with experimental observations at the later deformation stage. Fig. 10 shows the results for the plane-stress case. One can observe that the angle of the PLC bands to the tensile axis is about at 55° in the plane-stress case. Fig. 11 shows that the shear stress
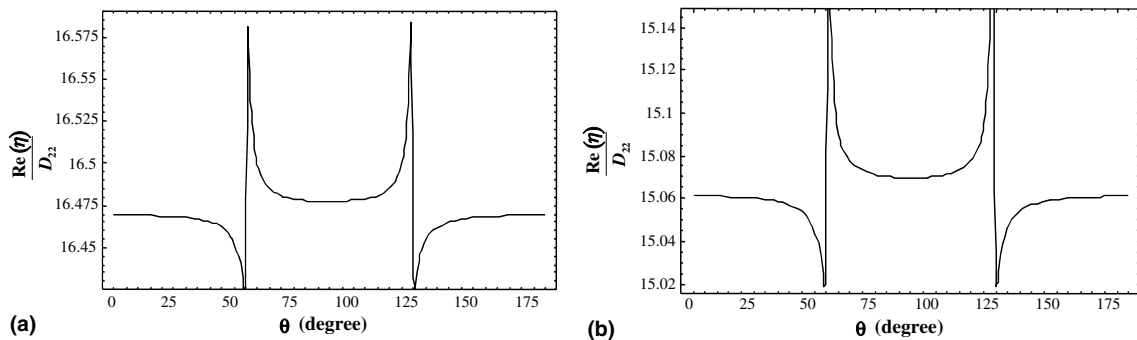

Fig. 10. Perturbation growth parameter at two different times in constrained model. Plane-stress case is considered. PLC band develops along two directions simultaneously. The angle between PLC bands and the tensile axis is about 60°, which is larger than in plane-strain case.
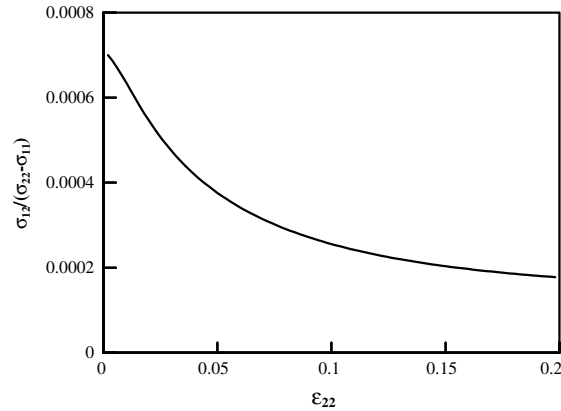
Fig. 11. Shear stress with respect to tensile strain in plane-strain case. Shear stress is very small compared to tensile stress, and the value decreases as the strain increases.

is very small compared to the normal stress in the uniaxial tension. The values for hardening modulus have been changed to examine the effect on the PLC band orientation, but they do not affect the results much.

In plane-strain case, the x_1 direction corresponds to the normal direction, and the specimen thickness along the x_1 direction is small. The surface of the specimen normal to the normal direction is usually observed in sheet metal forming. From our analysis for the plane-strain case, the PLC bands on the surface will be straight and parallel to the x_3 direction. When single bands form, the thickness of the PLC bands on the normal surface will be thin, and when the double bands develop, the PLC bands on the normal surface will be broad.

7. Concluding remarks

Boundary conditions and material inhomogeneity of polycrystalline metals have been considered to explain the spatial characteristics of the PLC bands associated with dynamic strain aging. It is believed that inclined bands appear when the material properties of tensile specimen are spatially inhomogeneous at the initial deformation stage, and the double bands appear when the material properties of tensile specimen have been spatially homogenized, and the shear rate of deformation vanishes at the later stage. These characters of initial and later deformation stages of polycrystalline metals were investigated by considering unconstrained and constrained models, and by changing initial material inhomogeneity. Tensile strain was decomposed into a duplex slip mode to account for the slipping in plastic deformation. By conducting a perturbation analysis and tracking the magnitude of stability parameters, it has been shown that single bands develop, when the system is not constrained, or the yield strength is inhomogeneous. A pair of symmetric double bands to the tensile axis develops, when the system is constrained, or the material property is spatially homogeneous. These results are in agreement with experimental observations of the PLC bands for AA6111-T4 sheet metal (Li, 2001). In plane-stress case, the angle of the PLC bands to the tensile axis turned out to be larger than in plane-strain case.

Biaxial tension is more useful in forming sheet metals by industry. Our perturbation analysis using slip modes to describe polycrystalline plastic deformation may be expanded to investigate the complex plasticity behavior of metals such as path-dependence and the Bauschinger effect.

Acknowledgements

Appendix A

The components of the matrix in (60) are given by

$$A_{1,1} = m\eta g_1^0 \frac{\left(\dot{\bar{\gamma}}_1^0\right)^{m-1}}{\dot{a}^m} e^{m\beta C_{s1}^0},$$

$$A_{1,3} = \left(\frac{\dot{\bar{\gamma}}_1^0}{\dot{a}}\right)^m e^{m\beta C_{s1}^0},$$

$$A_{1,5} = -\frac{1}{2} \sin 2\psi^0,$$

$$A_{1,6} = \begin{cases} \cos 2\psi^0 & \text{(PE)}, \\ \frac{1}{2} \cos 2\psi^0 & \text{(PS)}, \end{cases}$$

$$A_{1,9} = \begin{cases} -(\sigma_{22} - \sigma_{11})^0 \cos 2\psi^0 - 2\sigma_{12}^0 \sin 2\psi^0 & \text{(PE)}, \\ -\left(\sigma_{22} - \frac{1}{2}\sigma_{11}\right)^0 \cos 2\psi^0 - \sigma_{12}^0 \sin 2\psi^0 & \text{(PS)}, \end{cases}$$

$$A_{1,10} = m\beta g_1^0 \left(\frac{\dot{\bar{\gamma}}_1^0}{\dot{a}}\right)^m e^{m\beta C_{s1}^0},$$

$$A_{2,2} = m\eta g_2^0 \frac{\left(\dot{\bar{\gamma}}_2^0\right)^{m-1}}{\dot{a}^m} e^{m\beta C_{s2}^0},$$

$$A_{2,4} = \left(\frac{\dot{\bar{\gamma}}_2^0}{\dot{a}}\right)^m e^{m\beta C_{s2}^0},$$

$$A_{2,5} = -\frac{1}{2} \sin \left(4\phi - 2\psi^0\right),$$

$$A_{2,6} = \begin{cases} -\cos \left(4\phi - 2\psi^0\right) & \text{(PE)}, \\ -\frac{1}{2} \cos \left(4\phi - 2\psi^0\right) & \text{(PS)}, \end{cases}$$

$$A_{2,9} = \begin{cases} (\sigma_{22} - \sigma_{11})^0 \cos \left(4\phi - 2\psi^0\right) - 2\sigma_{12}^0 \sin \left(4\phi - 2\psi^0\right) & \text{(PE)}, \\ \left(\sigma_{22} - \frac{1}{2}\sigma_{11}\right)^0 \cos \left(4\phi - 2\psi^0\right) - \sigma_{12}^0 \sin \left(4\phi - 2\psi^0\right) & \text{(PS)}, \end{cases}$$

$$A_{2,10} = m\beta g_2^0 \left(\frac{\dot{\bar{\gamma}}_2^0}{a}\right)^m e^{m\beta C_{s2}^0},$$

$$A_{5,9} = 2\eta,$$

$$A_{5,14} = \eta,$$

$$A_{5,15} = -\eta,$$

$$A_{6,5} = n_1 n_2 \xi^2,$$

$$A_{6,6} = \begin{cases} \left(n_1^2 - n_2^2\right)\xi^2 & \text{(PE)}, \\ \left(n_1^2 - \frac{1}{2}n_2^2\right)\xi^2 & \text{(PS)}, \end{cases}$$

$$A_{7,7} = 2n_1\xi,$$

$$A_{7,9} = 2\left(\dot{\gamma}_1^0 \cos 2\psi^0 - \dot{\gamma}_2^0 \cos\left(4\phi - 2\psi^0\right)\right),$$

$$A_{7,14} = \eta \sin 2\psi^0,$$

$$A_{7,15} = \eta \sin\left(4\phi - 2\psi^0\right),$$

$$A_{8,7} = n_2\xi,$$

$$A_{8,8} = n_1\xi,$$

$$A_{8,9} = -2\left(\dot{\gamma}_1^0 \sin 2\psi^0 + \dot{\gamma}_2^0 \sin\left(4\phi - 2\psi^0\right)\right),$$

$$A_{8,14} = \eta \cos 2\psi^0,$$

$$A_{8,15} = -\eta \cos\left(4\phi - 2\psi^0\right),$$

$$A_{9,7} = \begin{cases} n_1\xi & \text{(PE)}, \\ 2n_1\xi & \text{(PS)}, \end{cases}$$

$$A_{10,14} = -\text{sign}\left(\dot{\gamma}_1^0\right),$$

$$A_{11,15} = -\text{sign}\left(\dot{\gamma}_2^0\right),$$

$$A_{12,12} = -\frac{2}{3}C_m\left(\frac{t_{w1}^0}{\tau}\right)^{\frac{-1}{3}} e^{-\left(\frac{t_{w1}^0}{\tau}\right)^{\frac{2}{3}}},$$

$$A_{13,13} = -\frac{2}{3}C_m\left(\frac{t_{w2}^0}{\tau}\right)^{\frac{-1}{3}} e^{-\left(\frac{t_{w2}^0}{\tau}\right)^{\frac{2}{3}}},$$

$$A_{14,1} = \frac{C}{\dot{\bar{\gamma}}_1^0} - \frac{C\eta\bar{\gamma}_1^0}{\left(\dot{\bar{\gamma}}_1^0\right)^2},$$

$$A_{15,2} = \frac{C}{\dot{\bar{\gamma}}_2^0} - \frac{C\eta\bar{\gamma}_2^0}{\left(\dot{\bar{\gamma}}_2^0\right)^2}.$$

PE stands for plane-strain, and PS stands for plane-stress. In this paper, $\text{sign}(\dot{\gamma}_1^0)$ and $\text{sign}(\dot{\gamma}_2^0)$ are positive, and the perturbation of the hardening modulus is neglected.

References

Bassani, J.L., 1994. Plastic flow of crystals. Adv. Appl. Mech. 30, 191–258.

Becker, R., 1999. Simulating effects of dynamic strain aging with a state variable model. In: Zabaras et al. (Eds.), The Integration of Material, Process and Product Design, pp. 77–84.

Dao, M., Asaro, R.J., 1996. Localized deformation modes and non-Schmid effects in crystalline solids. Part I. Critical conditions of localization. Mech. Mater. 23, 71–102.

Dieter, G.E., 1988. Mechanical Metallurgy. McGraw-Hill.

Dudzinski, D., Molinary, A., 1991. Perturbation analysis of thermoviscoplastic instabilities in axial loading. Int. J. Solids Struct. 27, 601–618.

Harren, S.V., Deve, H.E., Asaro, R.J., 1988. Shear band formation in plane strain compression. Acta Metall. 36, 2435–2480.

Khan, A., Huang, S., 1995. Continuum Theory of Plasticity. John Wiley & Sons, Inc.

Labbe, E., Hoc, T., Rey, C., 1998. A simplified crystallographic approach of bifurcation for single crystals and polycrystals. J. Phys. IV France 8, Pr8-215–Pr8-221.

Li, X., Tong, W., 1999. Characterization plastic strain inhomogeneity in thin metallic sheets. In: Multiscale Modeling of Materials I. Mater. Res. Soc. Proc. 538, 179–184.

Li, X., 2001. Spatial characterization and modeling of unstable plastic flow patterns in two aluminum alloys. Ph.D. Thesis, Yale University.

Smith, B.W., Li, X., Tong, W., 1998. Error assessment for strain mapping by digital image correlation. Exp. Tech. 22 (4), 19–21.

Tong, W., 1997. Detection of plastic deformation patterns in a binary aluminum alloy. Exp. Mech. 37 (4), 452–459.

Tong, W., 1998. Strain characterization of propagative deformation bands. J. Mech. Phys. Solids 46 (10), 2087–2102.

Yang, S.-Y., Tong, W., 2001. Interaction between dislocation and alloying elements and its implication on crystal plasticity of aluminum alloys. Mater. Sci. Eng. A 309–310, 300–303.

Zhang, S., McCormick, P.G., Estrin, Y., 2001. The morphology of Portevin–Le Chatelier bands: finite element simulation for Al–Mg–Si. Acta Mater. 49, 1087–1094.

Zikry, M.A., Pothier, M.R., Baucom, J.N., 2000. High strain-rate shear-strain localization in f.c.c. crystalline materials: a perturbation analysis. Int. J. Solids Struct. 37, 6177–6202.